Phys. Status Solidi B **254**, No. 8, 1600699 (2017) / **DOI** 10.1002/pssb.201600699

physica status solidi b
www.pss-b.com
basic solid state physics

100-nm thick single-phase wurtzite BAlN films with boron contents over 10%

Xiaohang Li[*,1,2], Shuo Wang[3], Hanxiao Liu[3], Fernando A. Ponce[3], Theeradetch Detchprohm[1], and Russell D. Dupuis[,1]**

[1] Center for Compound Semiconductors, School of Electrical and Computer Engineering, Georgia Institute of Technology, Atlanta, Georgia 30332, USA
[2] Computer, Electrical and Mathematical Sciences and Engineering Division, King Abdullah University of Science and Technology, Thuwal 23955, Saudi Arabia
[3] Department of Physics, Arizona State University, Tempe, Arizona 85287, USA

Received 23 October 2016, revised 27 November 2016, accepted 15 December 2016
Published online 17 January 2017

Keywords BAlN, boron, MOCVD, phases, wurtzite

[*] Corresponding author: e-mail xiaohang.li@kaust.edu.sa, Phone: +966-128087335
[**] e-mail dupuis@gatech.edu

Growing thicker BAlN films while maintaining single-phase wurtzite structure and boron content over 10% has been challenging. In this study, we report on the growth of 100 nm-thick single-phase wurtzite BAlN films with boron contents up to 14.4% by MOCVD. Flow-modulated epitaxy was employed to increase diffusion length of group-III atoms and reduce parasitic reactions between the metalorganics and NH_3. A large growth efficiency of $\sim$2000 μm mol^{-1} was achieved as a result. Small B/III ratios up to 17% in conjunction with high temperatures up to 1010 °C were utilized to prevent formation of the cubic phase and maintain wurtzite structure.

1 Introduction Because of compact size and potential reliability, deep UV (DUV) ($\lambda < 280$ nm) semiconductor lasers are expected to meet demands from non-line-of-sight communication, biochemical detection, and digital data storage. Due to the direct and appropriate bandgap energy, III-nitrides are suitable semiconductor materials for DUV lasers. Recently, low-threshold optically pumped edge-emitting lasers based on III-nitrides have been demonstrated, which is an important milestone towards realization of electrical-driven edge-emitting laser diodes [1, 2].

In comparison to the edge-emitting lasers, vertical-cavity surface-emitting lasers (VCSELs) possess desirable properties such as straightforward control of production process, high-speed modulation, and good beam quality. In spite of the development progress of edge-emitting DUV lasers, development of DUV VCSELs has been lagging. Recently, the onset of surface stimulated emission at 260 nm from AlGaN multiple quantum wells (MQWs) by optical pumping has been reported [3]. However, a true VCSEL requires distributed Bragg reflectors (DBRs) that are transparent and have reflectivity close to unity with sufficient bandwidth. Unfortunately, the reflectivity or bandwidth of III-nitride DUV DBRs based on AlGaN materials has been limited due to a limited change of refractive index as a function of the Al composition [4–6].

BAlN has been proposed as a promising material candidate for the high-reflectivity DBR [7, 8]. However, previous attempts of increasing the boron content for a larger index reduction via the epitaxial process only led to small boron contents of 1–2% in BAlN with the wurtzite structure [9], thereby limiting its application potential. Phase separation, short diffusion length of boron atoms, and strong parasitic reaction in the gas phase were attributed to the small boron contents. Recently, Li et al. reported on the growth of BAlN by a T-shape horizontal metalorganic chemical vapor deposition (MOCVD) reactor with a much higher boron content of 12% [10, 11]. However, the single-phase wurtzite structure was only observed in the first 10 nm or thinner region of the BAlN film. Beyond that, phase separation occurred with the presence of a highly tilted

cubic-like phase. This phase is undesirable in a wurtzite III-nitride device structure. The cause of the phase separation was not discussed but it is possible that the formation energy of the cubic phase is lower than that of wurtzite phase amid a large B/III molar flow ratio (hereafter "B/III ratio") of ~40%. Nevertheless, this growth condition may not be suitable for BAlN-based DBR structures where an individual wurtzite BAlN film needs to be around 30 nm thick in the DUV spectrum.

In this work, the considerably smaller B/III ratios up to 17% and flow-modulated epitaxy (FME) were employed at relatively high temperatures up to 1010 °C. We demonstrated BAlN layers with relatively high boron contents. The single-phase wurtzite structure was maintained throughout the entirety of 100-nm thickness of the BAlN films. Growth and characterization of two samples with different boron contents of 11.0 and 14.4% are presented.

2 Experimental Two 100-nm BAlN layers (hereafter "BAlN-I" and "BAlN-II") were grown on two *c*-plane AlN/sapphire templates under different conditions by a close-coupled showerhead (CCS) metalorganic chemical vapor deposition (MOCVD). The threading dislocation density of the AlN template layer was in the low $10^9/cm^2$ range and its surface was atomically smooth, providing a relatively good template quality for the BAlN growth [12]. Trimethylaluminum (TMA), triethylboron (TEB), and NH_3 were utilized as precursors. In the vapor phase, B/III ratios were kept at 12 and 17% for BAlN-I and BAlN-II, respectively, which are considerably lower than that (40%) of the previous reports [9, 11]. With reduced parasitic reaction between metalorganics and NH_3 and efficient incorporation, the boron contents should be higher than 10%.

To mitigate the parasitic reaction and increase diffusion length of group-III atoms to enhance B incorporation, FME was used, where the supplies of metalorganics and NH_3 were injected alternately into the growth chamber without interruption. To further mitigate the parasitic reaction, small V/III ratios of 58 and 39 were used for BAlN-I and BAlN-II in the vapor phase, respectively. Previously the suppression of parasitic reaction during the BAlN growth was studied [9, 10]. However, the growth efficiency of BAlN epitaxy has not been reported, making it difficult to evaluate the effect of the implemented methods. Based on the supplying molar flow rate of precursors and growth rate in this work, the growth efficiency of BAlN-I and BAlN-II was calculated to be ~2000 μm mol^{-1}, indicating that 31% of the injected group-III precursors was effectively incorporated to form the BAlN layer. This was similar to growth efficiencies of recent studies using small V/III ratios for efficient growth of AlN layers ([12, 13]). It indicated that the parasitic reactions were effectively suppressed under the current growth conditions.

Relatively high growth temperatures of 1010 and 910 °C were used for BAlN-I and BAlN-II, respectively, which aimed to increase the diffusion length of group-III atoms for better material quality. Although a further increased temperature is more desirable for the diffusion length and crystalline quality, we found that the B incorporation reduced if the temperature was too high. In particular, the impact of temperature on the reduction of B incorporation was found to be more severe when the B/III ratio was higher, probably due to enhanced parasitic reaction between TEB and NH_3.

3 Results and discussion The $5 \times 5\,\mu m^2$ atomic force microscopy (AFM) images of BAlN-I and BAlN-II are shown in Fig. 1(a) and (b), respectively. Both samples exhibited relatively smooth surfaces with RMS surface roughness of around 2 nm. But it is noted that columnar surface morphology was observed from both samples. It is possible that the initial growth was dominated by the Volmer–Weber (V–W) growth mode where a large number of surface nuclei were formed [14]. However, unlike conventional MOCVD of GaN where the initial V–W grow mode is followed by columnar growth and coalescence [15], these initial BAlN nuclei did not lead to island growth and subsequent lateral coalescence because the BAlN layers were still thin and the lateral growth rate was small. In addition, it is worth pointing out that the cross-sectional columnar diameter of BAlN-II (~130 nm) was larger than that of BAlN-I (~40 nm). Larger columns indicated higher lateral diffusivity of precursor atoms during the growth, which was probably due to a smaller V/III ratio of 39. More AFM studies are still needed especially at the first few nm of BAlN growth to provide a solid conclusion of the growth mode.

To probe the crystal structure, an X-ray diffraction (XRD) system equipped with a four-crystal monochromator ($4 \times$ Ge [220]) was employed by utilizing the Cu $K_{\alpha 1}$ line ($\lambda = 1.54$ Å). Figure 2(a) and (b) shows XRD (0002)-plane 2θ–ω scan spectra of the samples. Peaks of the two 100-nm BAlN layers were distinct without deconvolution, indicating wurtzite crystallinity was preserved. However, the relative peak intensity of BAlN-I was stronger than that of BAlN-II, indicating better wurtzite crystallinity. The 2θ angles of AlN and BAlN peaks of BAlN-I were 36.1398° and 36.4773°, respectively. The 2θ angles of AlN and BAlN peaks of BAlN-II were 36.1366° and 36.7175°, respectively. Thus

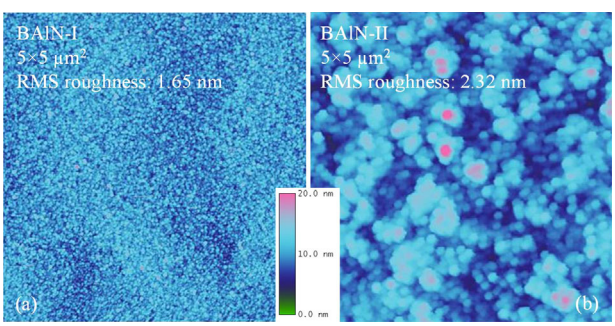

Figure 1 About $5 \times 5\,\mu m^2$ AFM images of (a) BAlN-I, (b) BAlN-II.

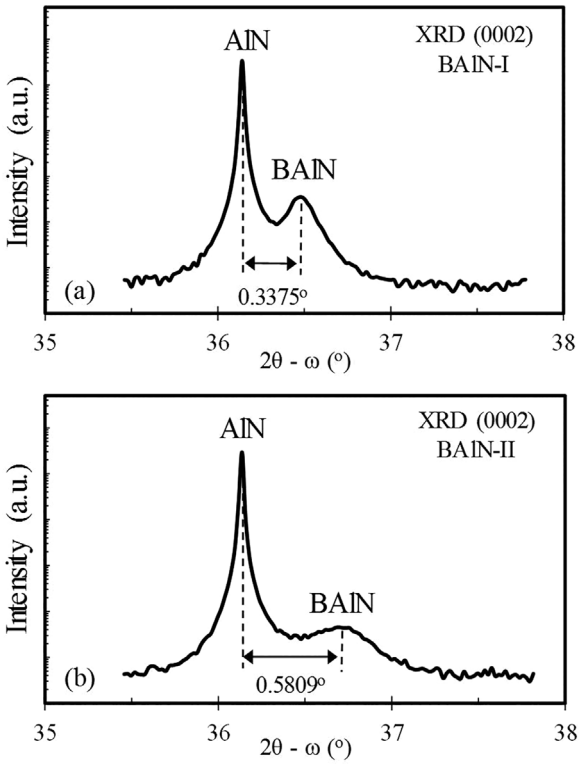

Figure 2 XRD (0002)-plane 2θ–ω scan spectra of (a) BAlN-I and (b) BAlN-II grown on the AlN/sapphire templates.

the 2θ angular separation of AlN-BAlN peaks of BAlN-I and BAlN-II were estimated to be 0.3375° and 0.5809°, respectively. This indicated the boron content of BAlN-II was larger due to the higher B/III ratio. According to the calculation of boron contents based on the Vegard's Law and Bragg's Law, the boron contents of BAlN-I and BAlN-II were estimated to be 5.9 and 10.2%, respectively. The lattice constant of wurtzite BN was from the study of Solozhenko et al. [16]. Reciprocal space mapping (RSM) measurement about the [10–15] diffraction plane was conducted, showing that the BAlN layers of BAlN-I and BAlN-II were pseudomorphically grown on the AlN template layers. In addition, the BAlN-related peak in the RSM is weak which could not yield the FWHM or lattice constants accurately. However, we expect the FWHM to be large given the high defect density shown in the transmission electron microscopy (TEM) images of Fig. 6. The asymmetric peak is weak and broad suggesting the columnar growth consistent with the TEM analysis.

It is known that the composition analysis by XRD can have errors due to lack of reported lattice parameters of BAlN with different compositions and material defects [10]. In this work, the Rutherford backscattering spectrometry (RBS) measurement and simulation were conducted by EAG Laboratories to determine the boron content. RBS is an accurate quantification tool for compositional analysis and is independent on strain and defect. RBS spectra were acquired at a grazing angle of ~108°. The samples were oriented perpendicular to the incident He^{++} ion beam with an energy of 2.275 MeV and slightly tilted to present a random geometry to the incident beam. That avoided channeling in both layers and substrate.

The RBS spectra of BAlN-I and BAlN-II are shown in Fig. 3(a) and (b), respectively. The boron peaks are visible. However, as boron has a small nucleus, the scattering cross section is small. Thus intensities of the boron peaks are weak. If the boron content is directly derived from the boron peaks, large errors are inevitable. However, the accurate aluminum contents can be obtained by simulation fitting because of distinct aluminum signals, from which the boron content can be derived as BAlN is ternary ([B] = 1 − [Al]). The fitting was conducted by the simulation program HYPRA of EAG Laboratories which is similar to RUMP [17]. Key fitting parameters including the channel 0 intercept (127.3 kV), energy per channel (4.37 kV/channel), and detector solid angle (2.67 msr) were applied [18]. The boron contents of BAlN-I and BAlN-II were determined to be 11.0 ± 2.0 and 14.4 ± 1.0%, respectively. Given the B/III ratios of 12 and 17% for BAlN-I and BAlN-II, respectively, the boron contents indicated that boron was efficiently incorporated into the BAlN films during the growth.

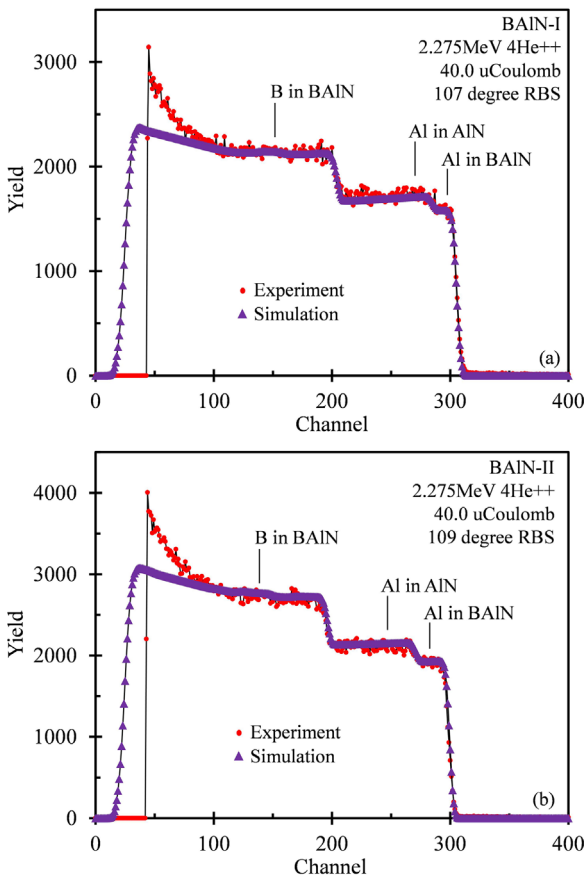

Figure 3 RBS spectra from experiment and simulation of (a) BAlN-I and (b) BAlN-II, respectively.

The crystal structure was firstly studied using cross-sectional high-resolution (HR) TEM along the $11\bar{2}0$ projection. The HR-TEM studies focused on the lower and upper portions of the 100-nm BAlN layers, respectively, which reflected the crystal microstructure and its evolution. The TEM specimens were prepared by mechanical wedge-polishing, followed by argon ion milling at 4.0 keV. As shown in Fig. 4(a) and (b), both lower and upper portions of BAlN-I show lattice oriented along *c*-axis, indicating that BAlN-I maintained good wurtzite crystallinity, which was consistent with the relatively strong BAlN peak observed in the XRD spectrum of Fig. 2(a).

In addition, Fig. 4(a) and (b) show a granular contrast variation, with the domain size on the order of 5–10 nm. The scale of this fluctuation is similar to the surface morphology. Thus we attributed it to a rough growth surface. Variation in the coherence depth (granular size) resulted in phase contrast where atoms varied in contrast between white and black, thus giving the impression of undulation in the (0002) planes. There are dark regions in the images, which we attribute to strong diffraction due to good alignment of the zone axis with respect to the electron beam. The wurtzite crystallinity of lower and upper portions was confirmed by the fast Fourier transform (FFT) diffraction patterns in Fig. 4(c) and (d).

A similar analysis was conducted for BAlN-II, which shows single wurtzite crystallinity of both upper and lower portions in Fig. 5(a)–(d). However, the upper portion of the film show a slight rotational variance in the diffraction pattern in Fig. 5(c), this is in the form of circular streaks. We attribute this to slight rotations of ± 2 degrees of the granular structure around $11\bar{2}0$ axes, with the wurtzite structure clearly preserved. This may be the cause for the weaker and broader BAlN peak in the XRD spectrum of Fig. 2(b) as compared to that of BAlN-I in Fig. 2(a).

Two factors may contribute to the slight rotation of lattice. First, a larger B/III ratio of 17% may lead to a reduction of the granular size and increase the probability of incomplete crystal alignment. This would need to be addressed by further optimizing the growth condition. Second, the increased tensile strain, introduced by the shorter B–N bonds compared to the Al–N bonds may further facilitate the rotation of small crystallites. This can be alleviated in the DBR by employing a strain-compensated structure.

To confirm wurtzite crystallinity, bright-field TEM diffraction contrast images were obtained for the entire BAlN layers of BAlN-I and BAlN-II, respectively, as shown in Fig. 6(a)–(b) and (d)–(e). The microstructure of these films was rich in defects. The images show vertical dark regions for $g = 0002$ and dark spots for $g = 1\bar{1}00$. We interpret the features for $g = 0002$ as fine columnar epitaxial growth, with strong *c*-axis orientation but with slight in-plane rotation that gives rise to vertical Moiré fringes which may be associated with screw dislocations. The dark spots for $g = 1\bar{1}00$ may be

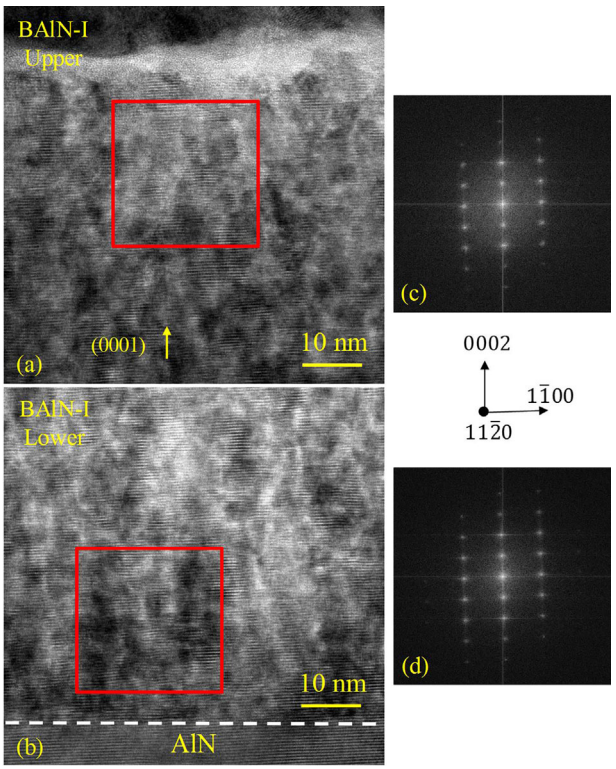

Figure 4 HR-TEM images of (a) upper and (b) lower portions and FFT diffraction patterns of randomly selected areas within the red squares of (c) upper and (d) lower portions of BAlN-I.

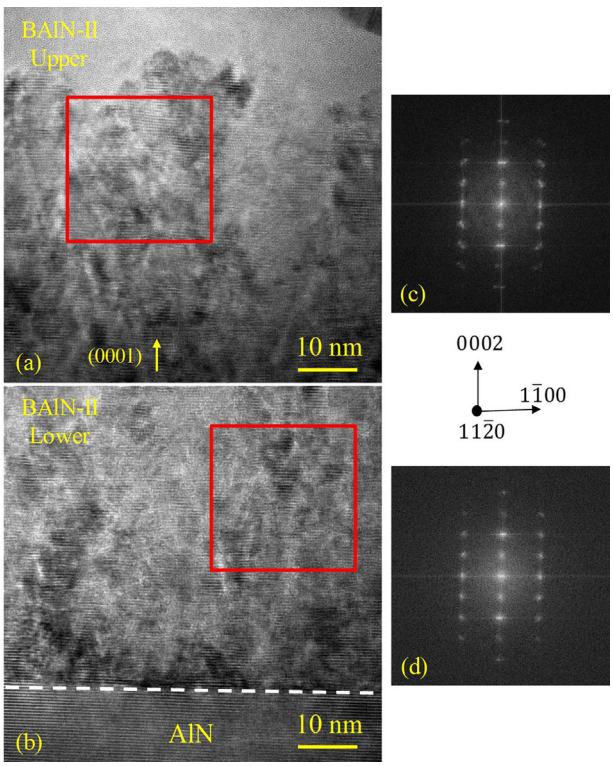

Figure 5 HR-TEM images of (a) upper and (b) lower portions and FFT diffraction patterns of randomly selected areas within the red squares of (c) upper and (d) lower portions of BAlN-II.

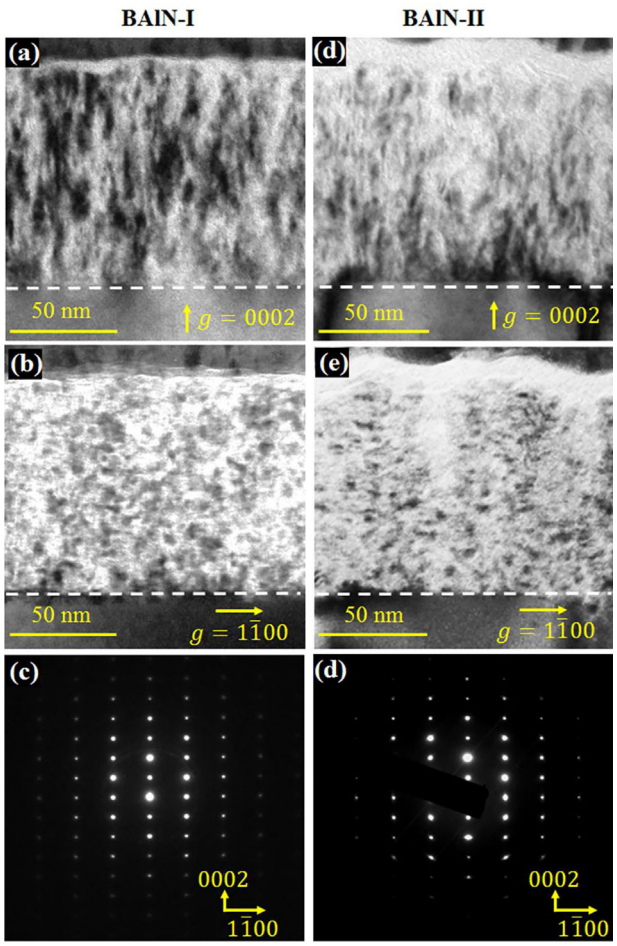

Figure 6 Cross-sectional bright-field TEM images taken under $g = 0002$ and $g = 1\bar{1}00$ conditions, and $11\bar{2}0$ diffraction patterns for (a)–(c) BAlN-I and (d)–(f) BAlN-II, respectively. The white dash lines represent the AlN/BAlN interface.

associated with the termination of columnar crystallites. Figure 6(c) and (f) shows $11\bar{2}0$ diffraction patterns of the entire BAlN layers of BAlN-I and BAlN-II, respectively, which manifest no evidence of other phases and are therefore consistent with the FFT diffraction patterns of the lower and upper regions (Figs. 4(c) and (d); 5(c) and (d)). Any significant variation in the composition of the BAlN film would appear as a streak in the diffraction pattern, which we did not observe. Hence, we conclude that the phase separation did not happen in both samples which maintained the wurtzite structure through the 100-nm thickness.

4 Conclusions In summary, we have demonstrated 100-nm single-phase wurtzite BAlN layers with boron contents over 10%. Relatively low B/III ratios up to 17% were used in conjunction with relatively high temperatures up to 1010 °C to prevent formation of highly tilted cubic phase to maintain single-phase wurtzite crystallinity. A large growth efficiency of $\sim 2000\ \mu m\ mol^{-1}$ was achieved as a result of the relatively small V/III ratios and FME.

Acknowledgements This work was supported by the U.S. National Science Foundation under DMR-1410874. RDD acknowledges support of the Steve W. Chaddick Endowed Chair in Electro-Optics and the Georgia Research Alliance. XL acknowledges support of the KAUST startup and baseline funding. The authors acknowledge beneficial discussion of RBS data with Dr. Daniel Tseng from EAG Laboratories.

References

[1] X. H. Li, T. T. Kao, M. Md. Satter, Y. O. Wei, S. Wang, H. Xie, S. C. Shen, P. D. Yoder, A. M. Fischer, F. A. Ponce, T. Detchprohm, and R. D. Dupuis, Appl. Phys. Lett. **106**, 041115 (2015).
[2] Z. Bryan, I. Bryan, S. Mita, J. Tweedie, Z. Sitar, and R. Collazo, Appl. Phys. Lett. **106**, 232101 (2015).
[3] X. Li, H. Xie, F. A. Ponce, J. H. Ryou, T. Detchprohm, and R. D. Dupuis, Appl. Phys. Lett. **107**, 241109 (2015).
[4] C. G. Moe, Y. Wu, J. Piprek, S. Keller, J. S. Speck, S. P. DenBaars, and D. Emerson, Phys. Status Solidi A **203**, 8 (2006).
[5] G. Brummer, D. Nothern, A. Yu. Nikiforov, and T. D. Moustakas, Appl. Phys. Lett. **106**, 221107 (2015).
[6] A. Franke, M. P. Hoffmann, R. Kirste, M. Bobea, J. Tweedie, F. Kaess, M. Gerhold, R. Collazo, and Z. Sitar, J. Appl. Phys. **120**, 135703 (2016).
[7] S. Watanabe, T. Takano, K. Jinen, J. Yamamoto, and H. Kawanishi, Phys. Status Solidi C **0**, 2691 (2003).
[8] M. Abid, T. Moudakir, G. Orsal, S. Gautier, A. En Naciri, Z. Djebbour, J.-H. Ryou, G. Patriarche, L. Largeau, H. J. Kim, Z. Lochner, K. Pantzas, D. Alamarguy, F. Jomard, R. D. Dupuis, J.-P. Salvestrini, P. L. Voss, and A. Ougazzaden, Appl. Phys. Lett. **100**, 051101 (2012).
[9] T. Akasaka and T. Makimoto, Appl. Phys. Lett. **88**, 041902 (2006).
[10] X. Li, S. Sundaram, Y. E. Gmili, T. Moudakir, F. Genty, S. Bouchoule, G. Patriarche, R. D. Dupuis, P. L. Voss, J. P. Salvestrini, and A. Ougazzaden, Phys. Status Solidi A **212**, 4 (2015).
[11] X. Li, S. Sundaram, Y. El Gmili, F. Genty, S. Bouchoule, G. Patriache, P. Disseix, F. Réveret, J. Leymarie, J.-P. Salvestrini, R. D. Dupuis, P. L. Voss, and A. Ougazzaden, J. Cryst. Growth **44**, 119 (2015).
[12] X. H. Li, S. Wang, H. Xie, Y. O. Wei, T. T. Kao, M. Md. Satter, S. C. Shen, P. D. Yoder, T. Detchprohm, R. D. Dupuis, A. M. Fischer, and F. A. Ponce, Phys. Status Solidi B **252**, 1089 (2015).
[13] A. Kakanakova-Georgieva, R. R. Ciechonski, U. Forsberg, A. Lundskog, and E. Janzen, Cryst. Growth Des. **9**, 880 (2009).
[14] M. Volmer and A. Weber, Z. Phys. Chem. **119**, 277 (1926).
[15] H. J. Scheel and T. Fukuda, Crystal Growth Technology (Wiley, Hoboken, NJ, 2003).
[16] L. V. Solozhenko, D. Häusermann, M. Mezouar, and M. Kunz, Appl. Phys. Lett. **72**, 1691 (1998).
[17] L. R. Doolittle, Nucl. Instrum. Methods B **9**, 344–351(1985).
[18] K. W. Chu, J. W. Mayer, and M. A. Nicolet, Backscattering Spectrometry (Academic Pres, New York, 1978).